
DSEG-LIME: IMPROVING IMAGE EXPLANATION BY HIERARCHICAL DATA-DRIVEN SEGMENTATION

Patrick Knab
 University of Mannheim
 Mannheim
 patrick.knab@uni-mannheim.de

Sascha Marton
 University of Mannheim
 Mannheim
 sascha.marton@uni-mannheim.de

Christian Bartelt
 University of Mannheim
 Mannheim
 christian.bartelt@uni-mannheim.de

ABSTRACT

Explainable Artificial Intelligence (XAI) is critical in unraveling decision-making processes in complex machine learning models. LIME (Local Interpretable Model-agnostic Explanations) is a well-known XAI framework for image analysis. It utilizes image segmentation to create features to identify relevant areas for classification. Consequently, poor segmentation can compromise the consistency of the *explanation* and undermine the importance of the segments, affecting the overall *interpretability*. Addressing these challenges, we introduce **DSEG-LIME** (Data-Driven Segmentation LIME), featuring: *i*) a *data-driven* segmentation for *human-recognized* feature generation by *foundation model* integration, and *ii*) a *hierarchical segmentation* procedure through *composition*. We benchmark DSEG-LIME on pre-trained models with images from the ImageNet classes - scenarios without domain-specific knowledge. Our findings demonstrate that DSEG outperforms in most of the XAI metrics and enhances the alignment of explanations with human-recognized concepts, significantly improving interpretability. The code is available under: <https://github.com/patrick-knab/DSEG-LIME>

Keywords Explainable AI (XAI) · Foundation Models · LIME

1 Introduction

Why should we trust you? Integration of AI-powered services into everyday scenarios, with or without the need for specific domain knowledge, is becoming increasingly common. An example is the *image* classification feature in smartphone photo galleries, which sorts images into various categories. For effective user engagement, accuracy and conformity to human understanding are crucial. Outsiders often want to evaluate these systems' performance post-deployment to quantify their functionality. For example, we might want to determine whether the AI accurately identifies various objects in a single gallery category. The derived question - 'Why should we *trust* the model?' - directly ties into the utility of *Local Interpretable Model-agnostic Explanations* (LIME) [1]. LIME seeks to demystify AI decision-making by identifying key features that influence the output of a model, underlying the importance of the Explainable AI (XAI) research domain, particularly when deploying opaque models in real-world scenarios [2, 3, 4].

Segmentation is key. LIME uses segmentation techniques to identify and generate features to determine the key areas of an image that are critical for classification. However, a challenge emerges when these segmentation methods highlight features that fail to align with identifiable, clear concepts or arbitrarily represent them. This issue is particularly prevalent with conventional segmentation techniques. These methods, often grounded in graph- or clustering-based approaches [11], were not initially designed for distinguishing between different objects within images. Yet, they are standard in LIME's implementation [1]. Additionally, these methods struggle with creating a *compositional object structure*, where objects, like a guitar, are identified by their components, such as the body or headstock, limiting segmentation clarity and relevance.

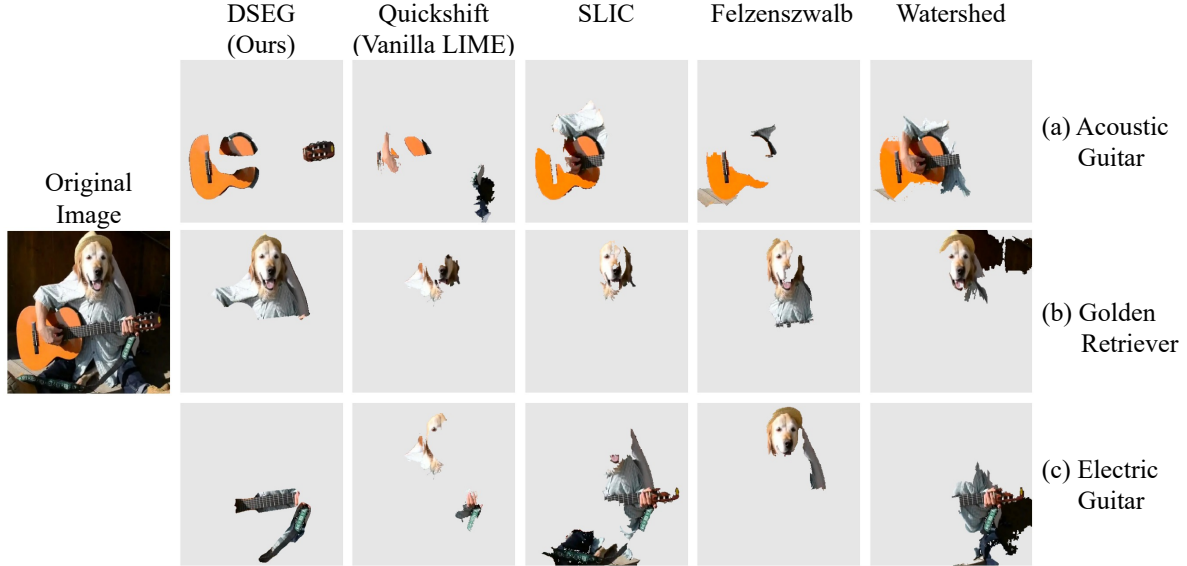


Figure 1: **Segmentation techniques within LIME.** Illustrating the explanations generated by LIME [1] for EfficientNetB4 [5], employing a variety of segmentation methods. These include DSEG (ours) combined with SAM (Segment Anything) [6], Quickshift [7], SLIC (Simple Linear Iterative Clustering) [8], Felzenszwalb [9] and the Watershed algorithm [10]. The top predictions are 'Acoustic Guitar' ($p = 0.31$), 'Golden Retriever' ($p = 0.24$), and 'Electric Guitar' ($p = 0.07$).

Ambiguous explanations. The composition of the segmentation has a significant influence on the explanation’s *quality* [12]. Images with a multitude of segments often exhibit notable *stability* issues within LIME (see Section 2), where it is not uncommon to encounter two entirely contradictory explanations for the same instance - eroding trust in both LIME’s explanation and the reliability of the model being analyzed [4, 13, 14, 15, 16]. Moreover, humans often struggle to *interpret* the explanations, as the highlighted areas do not align with our intuitive understanding [17, 18].

This work. In this paper, we address the challenges above by introducing **DSEG-LIME (Data-driven Segmentation LIME)**, an adaptation of the LIME framework for image analysis across domains where specialized knowledge is not required. We substitute the conventional segmentation algorithm with a transformer-based *foundation model*, SAM [6]. We frequently refer to these foundation models as *data-driven* to denote their ability to generate features that more accurately capture concepts recognizable by humans derived from vast imagery data collections. Given the great segmentation ability of SAM, we implement a compositional object structure, adapting LIME’s feature generation with a novel *hierarchical segmentation*. This adaptation provides flexibility in the granularity of concepts, allowing users to specify the detail of LIME’s explanation, viewing a car as a whole or in parts like doors and windshields. This approach breaks down broad categorizations, enabling independent evaluation of each sub-concept. Section 1 demonstrates the motivation mentioned above by employing LIME, which generates explanations using various segmentation techniques, specifically focusing on an image of a dog playing the guitar. In this context, DSEG excels by more clearly highlighting features that align with human-recognizable concepts, distinguishing it from other methods.

Contribution. In summary, the two main contributions of our paper are outlined as follows: *(i)* We introduce DSEG-LIME, which enhances the LIME framework for image analysis by integrating foundation models, particularly SAM, to improve feature quality and achieve more accurate explanations. *(ii)* DSEG advances LIME by incorporating a compositional object structure, enabling hierarchical segmentation, which allows for adjustable feature granularity.

To validate our claims, we extensively evaluate DSEG versus other segmentation methods and enhancements within the LIME framework across multiple pre-trained image classification models. We incorporate a user study for qualitative analysis and differentiate between explaining (*quantitative*) and interpreting (*qualitative*) aspects. Recognizing that the explanations considered most intuitive by users may not always align with the operational logic of the AI models, diverging from human perception [17, 19], we enhance our evaluation with various quantitative performance metrics widely used in XAI research [20].

2 Related work

In the following section, we briefly review related work, beginning with perturbation-based XAI methods and the stability issues of LIME. We then discuss studies on the influence of segmentation on explanations, concluding with techniques related to segmentation hierarchy.

Region-based perturbation XAI techniques. LIME is among several techniques designed to explain black box models through image perturbation. Fong and Vedaldi [21] introduced a meta-predictor framework that identifies critical regions via saliency maps. Subsequently, Fong et al. [22] developed the concept of extremal perturbations to address previous methods’ limitations. Additionally, Kapishnikov et al. [23] advanced an integrated-gradient, region-based attribution approach for more precise model explanations. More recently, Escudero-Viñolo et al. [24] have highlighted the constraints of perturbation-based explanations, advocating for the integration of semantic segmentation to enhance image interpretation.

Instability of LIME. The XAI community widely recognizes the instability in LIME’s explanations, which stems from LIME’s design [13, 14, 15, 16]. Alvarez-Melis and Jaakkola [13] handled this issue by showing the instability of various XAI techniques when slightly modifying the instance to be explained. A direct improvement is Stabilized-LIME (SLIME) proposed by Zhou et al. [14] based on the central limit theorem to approximate the number of perturbations needed in the data sampling approach to guarantee improved explanation stability. Zhau et al. [15] improved stability by exploiting prior knowledge and using Bayesian reasoning - BayLIME. GLIME [16] addressed this issue by employing an improved local and unbiased data sampling strategy, resulting in explanations with higher fidelity - similar to the work by Rashid et al. [25].

Segmentation influence on explanation. The segmentation algorithm utilized to sample data around the instance \mathbf{x} strongly influences its explanation. It directly affects the stability of LIME itself, as suggested by Chung et al. [26]. This behaviour is in line with the investigation by Schallner et al. [12] that examined the influence of different segmentation techniques in the medical domain, showing that the quality of the explanation depends on the underlying feature generation process. The work in [27] explored how occlusion and sampling strategies affect model explanations when integrated with segmentation techniques for XAI, including LRP (Layer-Wise Relevance Propagation) [28] and SHAP [29]. Their study highlights how different strategies provide unique explanations while evaluating the SAM technique in image segmentation. Sun et al. [30] used SAM within the SHAP framework to provide conceptually driven explanations.

Segmentation hierarchy. The work of Li et al. [31] aimed to simulate the way humans structure segments hierarchically and introduced a framework called Hierarchical Semantic Segmentation Networks (HSSN), which approaches segmentation through a pixel-wise multi-label classification task. HIPPIE (Hierarchical oPen-vocabulary, and unIvErsal segmentation), proposed by Wang et al. [32], extended hierarchical segmentation by merging text and image data multimodally. It processes inputs through decoders to extract and then fuse visual and text features into enhanced representations.

3 Foundations of LIME

In this section, we introduce the LIME framework [1], providing its theoretical foundation and functionality to establish the context for our approach.

Notation. We consider the scenario where we deal with imagery data. Let $\mathbf{x} \in \mathcal{X}$ represent an image within a set of images, and let $\mathbf{y} \in \mathcal{Y}$ denote its corresponding label in the output space with logits $\mathcal{Y} \subseteq \mathbb{R}$ indicating the labels in \mathcal{Y} . We denote the neural network we want to explain by $f : \mathcal{X} \rightarrow \mathcal{Y}$. This network functions by accepting an input \mathbf{x} and producing an output in \mathcal{Y} , which signifies the probability p of the instance being classified into a specific class.

3.1 Local Interpretable Model-agnostic Explanations

LIME is a prominent XAI framework designed to explain the decisions of a neural network f in a *model-agnostic* and *instance-specific* (local) manner. It applies to various modalities, including images, text, and tabular data [1]. In the following, we will briefly review LIME’s algorithm for treating images.

Feature generation. The technique involves training a local, interpretable surrogate model $g \in G$, where G is a class of interpretable models, such as linear models or decision trees, which approximates f ’s behavior around an instance \mathbf{x} [1]. This instance needs to be transformed into a set of features that can be used by g to compute the importance score of its features. In the domain of imagery data, segmentation algorithms segment \mathbf{x} into a set of superpixels $s_0 \dots s_d \in \mathcal{S}^D$, done by conventional techniques [7, 8, 9, 10]. We treat these superpixels as the features for which we calculate their

importance score. This step reflects the problematic process mentioned in Section 1, which forms the basis for the quality of the features that influence the explanatory quality of LIME.

Sample generation. For sample generation, the algorithm manipulates superpixels by toggling them randomly. Specifically, each superpixel s_i is assigned a binary state, indicating this feature’s visibility in a perturbed sample \mathbf{z} . The presence (1) or absence (0) of these features is represented in a binary vector \mathbf{z}'_i , where the i -th element corresponds to the state of the i -th superpixel in \mathbf{z} . When a feature s_i is absent (i.e., $s_i = 0$), its pixel values in \mathbf{z} are altered. This alteration typically involves replacing the original pixel values with a reference value, such as the mean pixel value of the image or a predefined value (e.g., black pixels) [1, 16]. Consequently, the modified instance \mathbf{z} , while retaining the overall structure of the original image \mathbf{x} , exhibits variations in its feature representation due to these alterations.

Feature attribution. LIME employs a proximity measure, denoted as $\pi_{\mathbf{x}}$, to assess the closeness between the predicted outputs $f(\mathbf{z})$ and $f(\mathbf{x})$, which is fundamental in assigning weights to the samples. In the standard implementation of LIME, the kernel $\pi_{\mathbf{x}}(\mathbf{z})$ is defined as follows:

$$\pi_{\mathbf{x}}(\mathbf{z}') = \exp\left(-\frac{D(\mathbf{x}', \mathbf{z}')^2}{\sigma^2}\right), \quad (1)$$

where \mathbf{x}' is a binary vector, all states are set to 1, representing the original image \mathbf{x} . D represents the $L2$ distance, given by $D(\mathbf{x}', \mathbf{z}') = \sqrt{\sum_{i=1}^n (\mathbf{x}'_i - \mathbf{z}'_i)^2}$ and σ being the width of the kernel. Subsequently, LIME trains a linear model, minimizing the loss function \mathcal{L} , which is defined as:

$$\mathcal{L}(f, g, \pi_{\mathbf{x}}) = \sum_{\mathbf{z}, \mathbf{z}' \in \mathcal{Z}} \pi_{\mathbf{x}}(\mathbf{z}) \cdot (f(\mathbf{z}) - g(\mathbf{z}'))^2 \quad (2)$$

In this equation, \mathbf{z} , and \mathbf{z}' are sampled instances from the perturbed dataset \mathcal{Z} , and g is the interpretable model being learned [1, 16]. The interpretability of the model is derived primarily from the coefficients of g . These coefficients quantify the influence of each feature on the model’s prediction, with each coefficient’s magnitude and direction (positive or negative) indicating the feature’s relative importance and effect.

4 DSEG-LIME

In this section, we will present DSEG-LIME’s two contributions: first, the substitution of traditional feature generation with a data-driven segmentation approach (Section 4.1), and second, the establishment of a hierarchical structure that organizes segments in a compositional manner (Section 4.2).

4.1 Data-driven segmentation integration

DSEG-LIME improves the LIME feature generation phase by incorporating data-driven transformer-based segmentation models, outperforming conventional graph- or cluster-based segmentation techniques in creating recognizable image segments across various domains. Specifically, our approach utilizes SAM (Segment Anything) [6] due to its remarkable capability to segment images across diverse areas. Figure 2 depicts the integration of DSEG within the LIME framework, following the processes outlined in Section 3. Here, the application of SAM in the feature generation phase influences the generation of superpixels/features \mathcal{S}^D , i.e. also \mathbf{z} and the binary vector \mathbf{z}' . Consequently, this change affects both the loss in Equation (2) and the proximity of the perturbed instances in Equation (1) that improves the approximation of an interpretable model g to explain \mathbf{x} of model f . We support this claim in the discussion of the experimental results.

4.2 Hierarchical segmentation

SAM’s segmentation capability, influenced by its design and hyperparameters, allows for both fine and coarse segmentations of an image [6]. The technique has the ability to segment a human-recognized concept at various levels, from the entirety of a car to its components, such as doors or windshields. This multitude of segments enables the composition of a concept into its sub-concepts, creating a hierarchical segmentation. We enhance the LIME framework by introducing hierarchical

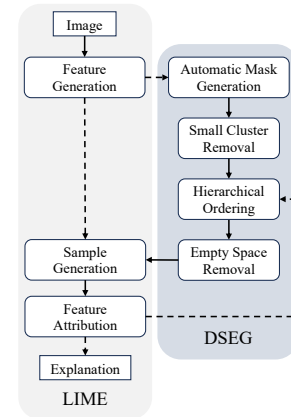


Figure 2: **Pipeline of DSEG in LIME.** Illustrating the LIME pipeline for image analysis with DSEG’s specific steps - dashed lines represent the choice between applying DSEG or not.

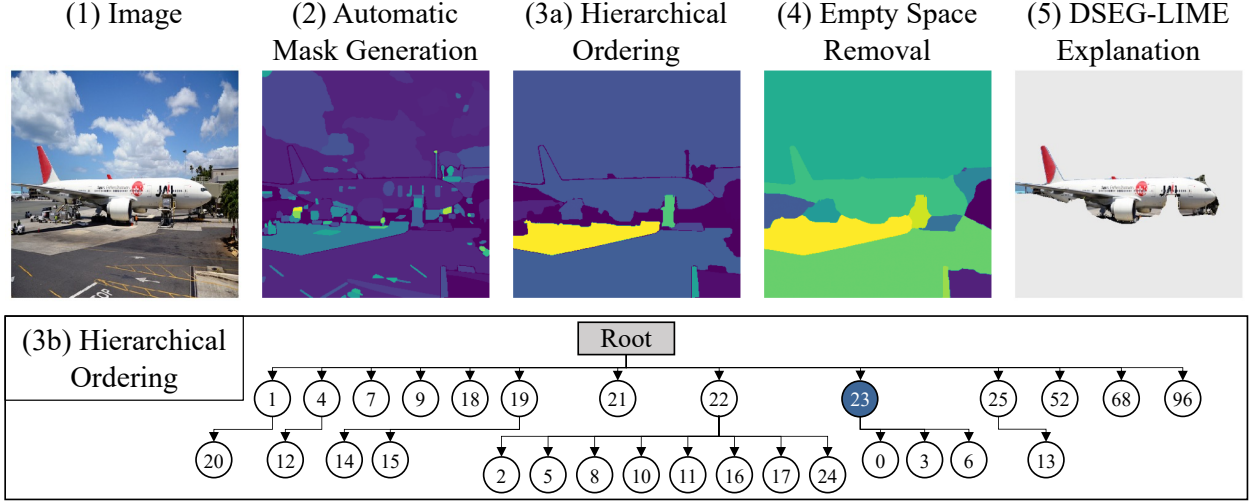


Figure 3: **Visualized DSEG pipeline.** Image (1) serves as the initial input, leading to its automatic segmentation depicted in (2). The hierarchical tree generated from this segmentation is illustrated in (3b), and (3a) showcases the mask composed of first-order nodes. Image (4) displays the finalized mask created after eliminating empty spaces, which is fed back into the sample generation of LIME. Image (5) represents the resultant explanation within the DSEG-LIME framework. The image shows an instance from the COCO dataset [33], classified as an 'Airliner' ($p = 0.86$) by EfficientNetB4. Node 23 (blue node) indicates the segment that represents the superpixel of the airliner.

segmentation, allowing users to specify segment granularity for more tailored explanations. The architecture allows the surrogate model to iteratively learn about features driven by human-recognizable concepts. DSEG starts by calculating the importance scores of coarse segments in the first stage. Segments identified as highly important are subsequently refined into their finer components, followed by another importance score calculation. Next, we detail the steps involved in DSEG (as illustrated in Figure 2) for explaining an image within the LIME framework, and Figure 3 shows the outputs of its intermediate steps.

Automatic mask generation. In the following, we denote the technique SAM by ζ . It can be used by prompting with points, marking areas, or automatically segmenting all visible elements in an image [6]. For DSEG, we utilize the last prompt, automated mask generation, since we want to segment the whole image for feature generation without human intervention. We express the process as follows:

$$M_{\text{auto}} = \zeta(\mathbf{x}, G_{\text{grid}}), \text{ with } \mathcal{S}^{\mathcal{D}} = M_{\text{auto}}, \quad (3)$$

where \mathbf{x} is the input image and G_{grid} is a grid overlay parameterized by the number of points per side, which facilitates automated segmentation. The output M_{auto} represents the automated mask generation, as illustrated Figure 3 (2).

Small cluster removal. SAM generates segments of varying sizes. We define a threshold θ such that segments with pixel-size below θ are excluded:

$$\mathcal{S}' = \{s_i \in \mathcal{S}^{\mathcal{D}} \mid \text{size}(s_i) \geq \theta\}. \quad (4)$$

In this study, we set $\theta = 500$ to reduce the feature set. The remaining superpixels in \mathcal{S}' are considered for feature attribution. SAM also allows the removal of small segments. But in DSEG, we enable user-driven segment exclusion post-processing, granting control over the granularity within the hierarchy and ensuring that users can adjust segmentation to their needs, thus enhancing the method's flexibility.

Hierarchical ordering. Given the fact of having overlapping segments, we impose a tree hierarchical structure $\mathcal{T} = (\mathcal{V}, \mathcal{E})$. The nodes $v \in \mathcal{V}$ denote segments in \mathcal{S}' , and the edges $(u, v) \in \mathcal{E}$ encode the hierarchical relationship between segments. This hierarchical ordering process $H(\mathcal{S}')$ is a composition of the relative overlap of the segments, defined as:

$$H(\mathcal{S}') = \text{BuildHierarchy}(\mathcal{S}', \text{OverlapMetric}), \quad (5)$$

where OverlapMetric quantifies the extent of overlap between two segments $s_1, s_2 \in \mathcal{S}'$ defined by

$$\text{OverlapMetric}(s_1, s_2) = \frac{|s_1 \cap s_2|}{|s_2|}. \quad (6)$$

The hierarchy prioritizes parent segments (e.g., person) over child segments (e.g., clothing), as depicted (3a) in Figure 3. Each node represents one superpixel with its unique identifier. The depth d of the hierarchy determines the granularity of the explanation, as defined by the user. A new set \mathcal{S}'_d , with $d = 1$, includes all nodes below the root. For $d > 1$, DSEG does not start from the beginning. Instead, it uses the segmentation hierarchy and segments \mathcal{S}' from the first iteration. It then adds the nodes of the children of the top k (a user-defined hyperparameter) most significant parent nodes in \mathcal{S}'_d at depth $d - 1$, identified during the feature attribution phase. We visualize this selection in the tree shown in Figure 3 (3b), where all nodes with depth one, including the children of node 23, are considered in the second iteration. For the scope of this paper, we concentrate on the first-order hierarchy ($d = 1$) but provide additional explanations with $d = 2$ in the Appendix A.3.

Empty space removal. In hierarchical segmentation, some regions occasionally remain unsegmented. We refer to these areas as R_{unseg} . To address this, we employ the nearest neighbor algorithm, which assigns each unsegmented region in R_{unseg} to the closest segment within the set \mathcal{S}'_d :

$$\mathcal{S}_d = \text{NearestNeighbor}(R_{\text{unseg}}, \mathcal{S}'_d). \quad (7)$$

Although this modifies the distinctiveness of concepts, it enhances DSEG-LIME’s explanatory power. DSEG then utilizes the features $s_0, \dots, s_d \in \mathcal{S}_d$ for feature attribution within LIME. Figure 3 (4) shows the corresponding mask along with the explanation of $d = 1$ in step (5) for the ‘airliner’ class.

5 Evaluation

In the following section, we will outline our experimental setup (Section 5.1) and introduce the XAI evaluation framework designed to assess DSEG-LIME both quantitatively (Section 5.2) and qualitatively (Section 5.3), compared to other LIME methodologies utilizing various segmentation algorithms. Subsequently, we discuss the limitations of DSEG (Section 5.4).

5.1 Experimental setup

Segmentation algorithms. Our experiment encompasses, along with SAM, four conventional segmentation techniques: *Simple Linear Iterative Clustering* (SLIC) [8], *Quickshift* (QS) [7], *Felzenszwalb* (FS) [9] and *Watershed* (WS) [10]. We carefully calibrate the hyperparameters of these techniques to produce segment counts similar to those generated by SAM. This calibration ensures that no technique is unfairly advantaged due to a specific segment count – for instance, scenarios where fewer but larger segments might yield better explanations than many smaller ones. We also integrated DETR (End-to-End Object Detection with Transformers) [34] into the DSEG approach to test an additional foundation model. However, this resulted in poorer performance, and we present and discuss the details in Appendix A.4.

Models to explain. The models investigated in this paper rely on pre-trained models, as our primary emphasis is on explainability. We chose EfficientNetB4 and EfficientNetB3 [5] as the ones treated in this paper, where we explain EfficientNetB4 and use EfficientNetB3 for a contrastivity check [20] (Section 5.2.1). To verify that our approach works on arbitrary pre-trained models, we also evaluated it using ResNet-101 [35, 36] and VisionTransformer (ViT-384) [37]. Detailed results of these tests are given in Appendices A.1 and A.2.

Dataset. We use images from the ImageNet classes [38], on which the models we investigate were trained [5, 35, 37]. Our final dataset consists of 20 carefully selected instances (see Appendix B.1), specifically chosen to comprehensively evaluate the techniques, both quantitatively and qualitatively. However, we want to emphasize that the selection of images is not biased toward any model.

Hyperparameters and hardware setup. The experiments were conducted on an Nvidia RTX A6000 GPU with 48 GB of VRAM, supported by a CPU with 1024 GB of RAM. We compare standard LIME, SLIME [14], GLIME [16], and BayLIME [15], all integrated with DSEG, using 256 samples per instance and a batch size of ten. For each explanation, up to three features are selected based on their significance, identified by values that exceed the average by more than 1.5 times the standard deviation. In BayLIME, we use the ‘non-info-prior’ setting. For SAM, we configure it to use 32 points per side, and the conventional segmentation techniques are adjusted to achieve a similar segment count, as previously mentioned. In SLIC, we modify the number of segments and compactness; in Quickshift, the kernel size and maximum distance; in Felzenszwalb, the scale of the minimum size parameter; and in Watershed, the number of markers and compactness. Other hyperparameters remain at default settings to ensure a balanced evaluation across methods.

5.2 Quantitative evaluation

We adapt the framework by Nauta et al. [20] to quantitatively assess XAI outcomes in this study, covering three domains: *content*, *presentation*, and *user experience*. In the content domain, we evaluate *correctness*, *output completeness*, *consistency*, and *contrastivity*. Presentation domain metrics like *compactness* and *confidence* are assessed under content for simplicity. We will briefly describe each metric individually to interpret the results correctly. The user domain, detailed in Section 5.3, includes a user study that compares our approach with other segmentation techniques in LIME. We use quantitative and qualitative assessments to avoid over-emphasizing technical precision or intuitive clarity [17].

5.2.1 Quantitative metrics definition

Correctness involves two randomization checks. The *model randomization parameter check* (Random Model) [39] tests if changing the random model parameters leads to different explanations. The *explanation randomization check* (Random Expl.) [40] examines if random output variations in the predictive model yield various explanations. For both metrics, in Table 1 we count the instances where explanations result in different predictions when reintroduced into the model under analysis. The domain also utilizes two deletion techniques: *single deletion* [41] and *incremental deletion* [7, 42]. *Single deletion* serves as an alternative metric to assess the completeness of the explanation, replacing less relevant superpixels with a specific background to evaluate their impact on the model predictions [43]. After these adjustments, we note instances where the model maintains the correct image classification. *Incremental deletion* (Incr. Deletion) entails progressively eliminating features from most to least significant based on their explanatory importance. We observe the model’s output variations, quantifying the impact by measuring the area under the curve (AUC) of the model’s confidence, as parts of the explanation are excluded. This continues until a classification change is observed (not ground truth class), and the mean AUC score for this metric is documented in Table 2.

Output completeness measures whether an explanation covers the crucial area for accurate classification. It includes a *preservation check* (Preservation) [42] to assess whether the explanation alone upholds the original decision, and a *deletion check* (Deletion) [44] to evaluate the effect of excluding the explanation on the prediction outcome [43]. This approach assesses both the completeness of the explanation and its impact on the classification. The results are checked to ensure that the consistency of the classification is maintained. *Compactness* is also considered, highlighting that the explanation should be concise and cover all the areas necessary for prediction [45], reported by the mean value.

Consistency assesses explanation robustness to minor input alterations, like Gaussian noise addition, by comparing pre- and post-perturbation explanations for *stability against slight changes* (Noise Stability) [46, 47], using both preservation and deletion checks. For consistency of the feature importance score, we generate explanations for the same instance eight times (Rep. Stability), calculate the standard deviation σ_i for each coefficient i , and then average all σ_i values. This yields $\bar{\sigma}$, the average standard deviation of coefficients, and is reported as the mean score.

Contrastivity integrates several previously discussed metrics, aiming for *target-discriminative* explanations. This means that an explanation e_x for an instance x from a primary model f_1 (EfficientNetB4) should allow a secondary model f_2 (EfficientNetB3) to mimic the output of f_1 as $f_1(x) \approx f_2(e_x)$ [48]. The approach checks the explanation’s utility and transferability across models, using EfficientNetB3 for preservation and deletion tests to assess consistency.

5.2.2 Quantitative evaluation results

Table 1 presents the outcomes of all metrics associated with class-discriminative outputs. The numbers in bold signify the top results, with an optimal score of 20. We compare LIME (L) [1] with the LIME techniques discussed in Section 2, SLIME (S) [14], GLIME (G) [16], and BayLIME (B) [15] in combination with DSEG and the segmentation techniques from Section 5.1. The randomization checks in the correctness category confirm that the segmentation algorithm bias does not inherently affect any model. This is supported by the observation that most methods correctly misclassify when noise is introduced or when the model’s weights or predictions are shuffled. In contrast, DSEG excels in other metrics, surpassing alternative methods regardless of the LIME technique applied. In the output completeness domain, DSEG’s explanations more effectively capture the critical areas necessary for the model to accurately classify an instance, whether by isolating or excluding the explanation. This efficacy is supported by the single deletion metric, akin to the preservation check but with a perturbed background. Moreover, noise does not compromise the consistency of DSEG’s explanations. The contrastivity metric demonstrates DSEG’s effectiveness in creating explanations that allow another AI model to produce similar outputs in over half of the cases and outperform alternative segmentation approaches. Overall, the influence of the LIME feature attribution calculation does not vary much, but this is because we do not exceed 44 segments in the covered dataset for evaluation due to object-driven segmentation with a hierarchy depth of one.

Table 2 further demonstrates the proficiency of DSEG in capturing crucial areas for model output, particularly with incremental deletion where SLIME and GLIME lead—the numbers in bold stand for the lowest value, which indicates

Table 1: **Quantitative summary - classes.** The table presents four quantitative areas and their metrics, comparing five segmentation techniques applied to EfficientNetB4: DSEG with SAM and comparative methods SLIC, Quickshift (QS), Felzenszwalb’s (FS), and Watershed (WS). We test each with four LIME framework variations: LIME (L), SLIME (S), GLIME (G), and BayLIME (B). The experimental setup and metrics are detailed in Section 5.1 and Section 5.2.1. The table includes class-based metrics, with a maximum score of 20 for each; higher scores indicate better performance, and the highest scores for each metric are highlighted in bold.

Domain	Metric	DSEG				SLIC				QS				FS				WS			
		L	S	G	B	L	S	G	B	L	S	G	B	L	S	G	B	L	S	G	B
Correctness	Random Model ↑	14	14	14	14	14	14	14	14	15	15	15	15	14	14	14	14	13	13	13	13
	Random Expl. ↑	13	17	18	19	15	19	16	15	17	16	15	16	19	18	18	15	14	16	16	14
	Single Deletion ↑	14	14	14	14	8	8	8	8	6	7	5	6	8	8	9	8	6	7	7	5
Output Completeness	Preservation ↑	17	17	17	18	16	16	16	16	12	12	13	13	14	14	14	14	15	15	15	15
	Deletion ↑	14	13	13	13	7	8	8	8	5	5	5	5	9	9	9	9	10	10	10	10
Consistency	Noise Stability ↑	17	17	16	17	14	14	14	14	9	10	9	10	15	14	15	15	14	14	14	13
Contrastivity	Preservation ↑	12	11	11	11	9	9	9	9	6	6	6	6	10	10	10	10	11	11	11	11
	Deletion ↑	14	13	13	13	9	10	10	10	10	10	10	10	10	10	10	10	9	9	9	9

the best performance. Although compactness metrics show nearly uniform segment sizes across the techniques, Watershed’s smaller segments do not translate to better performance in other areas. Repeated experimentation suggests that stability is less influenced by the LIME variant and more by the segmentation approach, with SLIC and DSEG outperforming others. Further experiments show that DSEG outperforms SLIC in terms of stability as the number of features increases. This advantage arises from the tendency of data-driven approaches to represent known objects uniformly as a single superpixel. Thus, if a superpixel accurately reflects the instance that the model in question predicts, it can be accurately and effortlessly matched with one or a few superpixels - such accurate matching leads to a more precise and more reliable explanation. Conventional segmentation algorithms often divide the same area into multiple superpixels, creating unclear boundaries and confusing differentiation between objects. The segmentation phase is the main differentiator regarding computation time; DSEG has longer processing times than the others. Nevertheless, it is essential to note that computation time is also subject to the server load where the experiments were conducted, thereby introducing the possibility of slight variations.

5.3 Qualitative evaluation

User study. Following the methodology by Chromik and Schuessler [49], we carried out a user study (approved by the institute’s ethics council) to assess the interpretability of the explanations. This study involved 87 participants recruited via Amazon Mechanical Turk (MTurk), encompassing all 20 images in our dataset (see Appendix B.1). These images were accompanied by explanations using DSEG and other segmentation techniques within the LIME framework (see Section 5.1).

Table 3: **User study results.** This table summarizes each segmentation approach’s average scores and top-rated counts of the user study results.

Metric	DSEG	SLIC	QS	FS	WS
Avg. Score ↑	4.16	3.01	1.99	3.25	2.59
Best Rated ↑	1042	150	90	253	205

Table 2: **Quantitative summary - numbers.** The table summarizes metrics from Section 5.2.1, focusing on those quantified by rational numbers like incremental deletion, compactness, representational stability, and average computation time across 20 examples, detailed in Section 5.1. In contrast to Table 1, lower values indicate better performance and the lowest values are printed in bold.

Metric	DSEG				SLIC				QS				FS				WS			
	L	S	G	B	L	S	G	B	L	S	G	B	L	S	G	B	L	S	G	B
Incr. Deletion ↓	0.33	0.18	0.19	0.34	0.38	0.31	0.30	0.35	0.43	0.44	0.44	0.41	0.40	0.42	0.45	0.43	0.32	0.36	0.36	0.32
Compactness ↓	0.12	0.13	0.13	0.13	0.13	0.13	0.13	0.13	0.12	0.13	0.13	0.14	0.14	0.14	0.14	0.14	0.10	0.11	0.10	0.11
Rep. Stability ↓	.008	.009	.009	.009	.008	.008	.009	.009	.011	.011	.012	.011	.011	.010	.011	.010	.012	.012	.012	.012
Time ↓	45.6	50.3	45.8	50.8	17.8	18.1	19.5	17.6	28.9	26.1	25.9	25.5	17.4	18.6	18.8	18.6	16.9	17.9	19.8	17.3

Participants rated the explanations on a scale from 1 (least effective) to 5 (most effective) based on their intuitive understanding and the predicted class. Table 3 summarizes the average scores, the cumulative number of top-rated explanations per instance, and the statistical significance of user study results for each segmentation approach. DSEG is most frequently rated as the best and consistently ranks high even when it is not the leading explanation. Paired t-tests indicate that DSEG is statistically significantly superior (additional results in Appendix B.2).

5.4 Limitations and future work

DSEG-LIME performs the feature generation directly on images before they are input into the model for explanation. For models like ResNet with smaller input sizes [35], the quantitative advantages of DSEG are less evident (see Appendix A.1. Furthermore, substituting superpixels with a specific value in preservation and deletion evaluations can introduce an inductive bias [4]. To reduce this bias, using a generative model to synthesize replacement areas could offer a more neutral alteration. Lastly, our approach, like any other LIME-based method [1, 14, 15, 16], does not assume a perfect match between the explanation domains and the model’s actual domains since it simplifies the model by a local surrogate. Nonetheless, our quantitative analysis confirms that the approximations closely reflect the model’s behavior. Future work could focus on integrating the foundation model directly into the system through a model-intrinsic approach, similar to [30].

No free lunch. Although DSEG provides promising results in many domains, it is not always universally applicable. When domain-specific knowledge is crucial to identify meaningful features or the feature generation task is inherently complex, DSEG might not perform as effectively as traditional segmentation methods within LIME [50] (Appendix A.5). However, future exploration could involve testing alternative segmentation techniques, such as integrating HSSN [32] or HIPPIE [31] instead of SAM (or DETR) to overcome this limitation.

6 Conclusion

In this study, we introduced DSEG-LIME, an extension to the LIME framework, incorporating a data-driven foundation model (SAM) for feature generation. This approach ensures that the generated features more accurately reflect human-recognizable concepts, enhancing the interpretability of explanations. Furthermore, we refined the process of feature attribution within LIME through an iterative method, establishing a segmentation hierarchy that contains the relationships between components and their subcomponents. Through a comprehensive two-part evaluation, split into quantitative and qualitative analysis, DSEG emerged as the superior method, outperforming other LIME-based approaches in most evaluated metrics. The adoption of foundational models marks a significant step towards enhancing the interpretability of deep learning models.

References

- [1] Marco Tulio Ribeiro, Sameer Singh, and Carlos Guestrin. "why should i trust you?": Explaining the predictions of any classifier. In *Proceedings of the 22nd ACM SIGKDD International Conference on Knowledge Discovery and Data Mining*, KDD '16, page 1135–1144, New York, NY, USA, 2016. Association for Computing Machinery.
- [2] Alejandro Barredo Arrieta, Natalia Díaz-Rodríguez, Javier Del Ser, Adrien Bannetot, Siham Tabik, Alberto Barbado, Salvador Garcia, Sergio Gil-Lopez, Daniel Molina, Richard Benjamins, Raja Chatila, and Francisco Herrera. Explainable artificial intelligence (xai): Concepts, taxonomies, opportunities and challenges toward responsible ai. *Information Fusion*, 58:82–115, 2020.
- [3] Pantelis Linardatos, Vasilis Papastefanopoulos, and Sotiris Kotsiantis. Explainable ai: A review of machine learning interpretability methods. *Entropy*, 23(1), 2021.
- [4] Damien Garreau and Dina Mardaoui. What does lime really see in images? In *International Conference on Machine Learning*, 2021.
- [5] Mingxing Tan and Quoc Le. Efficientnet: Rethinking model scaling for convolutional neural networks. In *International conference on machine learning*, pages 6105–6114. PMLR, 2019.
- [6] Alexander Kirillov, Eric Mintun, Nikhila Ravi, Hanzi Mao, Chloe Rolland, Laura Gustafson, Tete Xiao, Spencer Whitehead, Alexander C. Berg, Wan-Yen Lo, Piotr Dollár, and Ross Girshick. Segment anything, 2023.
- [7] Lukas Hoyer, Mauricio Munoz, Prateek Katiyar, Anna Khoreva, and Volker Fischer. Grid saliency for context explanations of semantic segmentation. In H. Wallach, H. Larochelle, A. Beygelzimer, F. d'Alché-Buc, E. Fox, and R. Garnett, editors, *Advances in Neural Information Processing Systems*, volume 32. Curran Associates, Inc., 2019.

- [8] Radhakrishna Achanta, Appu Shaji, Kevin Smith, Aurelien Lucchi, Pascal Fua, and Sabine Süsstrunk. Slic superpixels compared to state-of-the-art superpixel methods. *IEEE Transactions on Pattern Analysis and Machine Intelligence*, 34(11):2274–2282, 2012.
- [9] Pedro F. Felzenszwalb and Daniel P. Huttenlocher. Efficient graph-based image segmentation. *International Journal of Computer Vision*, 59:167–181, 2004.
- [10] Peer Neubert and Peter Protzel. Compact watershed and preemptive slic: On improving trade-offs of superpixel segmentation algorithms. In *2014 22nd International Conference on Pattern Recognition*, pages 996–1001, 2014.
- [11] Murong Wang, Xiabi Liu, Yixuan Gao, Xiao Ma, and Nouman Q. Soomro. Superpixel segmentation: A benchmark. *Signal Processing: Image Communication*, 56:28–39, 2017.
- [12] Ludwig Schallner, Johannes Rabold, Oliver Scholz, and Ute Schmid. Effect of superpixel aggregation on explanations in lime – a case study with biological data. In Peggy Cellier and Kurt Driessens, editors, *Machine Learning and Knowledge Discovery in Databases*, pages 147–158, Cham, 2020. Springer International Publishing.
- [13] David Alvarez-Melis and Tommi S. Jaakkola. On the robustness of interpretability methods. *CoRR*, abs/1806.08049, 2018.
- [14] Zhengze Zhou, Giles Hooker, and Fei Wang. S-lime: Stabilized-lime for model explanation. In *Proceedings of the 27th ACM SIGKDD Conference on Knowledge Discovery & Data Mining, KDD ’21*, page 2429–2438, New York, NY, USA, 2021. Association for Computing Machinery.
- [15] Xingyu Zhao, Xiaowei Huang, V. Robu, and David Flynn. Baylime: Bayesian local interpretable model-agnostic explanations. In *Conference on Uncertainty in Artificial Intelligence*, 2020.
- [16] Zeren Tan, Yang Tian, and Jian Li. Glime: General, stable and local lime explanation. *Advances in Neural Information Processing Systems*, 36, 2024.
- [17] Christoph Molnar, Gunnar König, Julia Herbringer, Timo Freiesleben, Susanne Dandl, Christian A. Scholbeck, Giuseppe Casalicchio, Moritz Grosse-Wentrup, and Bernd Bischl. General pitfalls of model-agnostic interpretation methods for machine learning models. In Andreas Holzinger, Randy Goebel, Ruth Fong, Taesup Moon, Klaus-Robert Müller, and Wojciech Samek, editors, *xxAI - Beyond Explainable AI: International Workshop, Held in Conjunction with ICML 2020, July 18, 2020, Vienna, Austria, Revised and Extended Papers*, pages 39–68, Cham, 2022. Springer International Publishing.
- [18] Sunnie SY Kim, Nicole Meister, Vikram V Ramaswamy, Ruth Fong, and Olga Russakovsky. Hive: Evaluating the human interpretability of visual explanations. In *European Conference on Computer Vision*, pages 280–298. Springer, 2022.
- [19] Timo Freiesleben and Gunnar König. Dear xai community, we need to talk! fundamental misconceptions in current xai research, 2023.
- [20] Meike Nauta, Jan Trienes, Shreyasi Pathak, Elisa Nguyen, Michelle Peters, Yasmin Schmitt, Jörg Schlötterer, Maurice van Keulen, and Christin Seifert. From anecdotal evidence to quantitative evaluation methods: A systematic review on evaluating explainable ai. *ACM Comput. Surv.*, 55(13s), jul 2023.
- [21] Ruth C Fong and Andrea Vedaldi. Interpretable explanations of black boxes by meaningful perturbation. In *Proceedings of the IEEE international conference on computer vision*, pages 3429–3437, 2017.
- [22] Ruth Fong, Mandela Patrick, and Andrea Vedaldi. Understanding deep networks via extremal perturbations and smooth masks. In *Proceedings of the IEEE/CVF international conference on computer vision*, pages 2950–2958, 2019.
- [23] Andrei Kapishnikov, Tolga Bolukbasi, Fernanda Viégas, and Michael Terry. Xrai: Better attributions through regions. In *Proceedings of the IEEE/CVF international conference on computer vision*, pages 4948–4957, 2019.
- [24] Marcos Escudero-Viñolo, Jesús Bescós, Alejandro López-Cifuentes, and Andrija Gajić. Characterizing a scene recognition model by identifying the effect of input features via semantic-wise attribution. In *Explainable Deep Learning AI*, pages 55–77. Elsevier, 2023.
- [25] Muhammad Rashid, Elvio G. Amparore, Enrico Ferrari, and Damiano Verda. Using stratified sampling to improve lime image explanations. *Proceedings of the AAAI Conference on Artificial Intelligence*, 38(13):14785–14792, Mar. 2024.
- [26] Chung Hou Ng, Hussain Sadiq Abuwala, and Chern Hong Lim. Towards more stable lime for explainable ai. In *2022 International Symposium on Intelligent Signal Processing and Communication Systems (ISPACS)*, pages 1–4, 2022.
- [27] Stefan Blücher, Johanna Vielhaben, and Nils Strodthoff. Decoupling pixel flipping and occlusion strategy for consistent xai benchmarks, 2024.

- [28] Grégoire Montavon, Alexander Binder, Sebastian Lapuschkin, Wojciech Samek, and Klaus-Robert Müller. *Layer-Wise Relevance Propagation: An Overview*, pages 193–209. Springer International Publishing, Cham, 2019.
- [29] Scott M. Lundberg and Su-In Lee. A unified approach to interpreting model predictions. In *Proceedings of the 31st International Conference on Neural Information Processing Systems*, NIPS’17, page 4768–4777, Red Hook, NY, USA, 2017. Curran Associates Inc.
- [30] Ao Sun, Pingchuan Ma, Yuanyuan Yuan, and Shuai Wang. Explain any concept: Segment anything meets concept-based explanation, 2023.
- [31] Liulei Li, Tianfei Zhou, Wenguan Wang, Jianwu Li, and Yi Yang. Deep hierarchical semantic segmentation. In *Proceedings of the IEEE/CVF Conference on Computer Vision and Pattern Recognition*, pages 1246–1257, 2022.
- [32] Xudong Wang, Shufan Li, Konstantinos Kallidromitis, Yusuke Kato, Kazuki Kozuka, and Trevor Darrell. Hierarchical open-vocabulary universal image segmentation. In A. Oh, T. Neumann, A. Globerson, K. Saenko, M. Hardt, and S. Levine, editors, *Advances in Neural Information Processing Systems*, volume 36, pages 21429–21453. Curran Associates, Inc., 2023.
- [33] Tsung-Yi Lin, Michael Maire, Serge Belongie, James Hays, Pietro Perona, Deva Ramanan, Piotr Dollár, and C. Lawrence Zitnick. Microsoft coco: Common objects in context. In David Fleet, Tomas Pajdla, Bernt Schiele, and Tinne Tuytelaars, editors, *Computer Vision – ECCV 2014*, pages 740–755, Cham, 2014. Springer International Publishing.
- [34] Nicolas Carion, Francisco Massa, Gabriel Synnaeve, Nicolas Usunier, Alexander Kirillov, and Sergey Zagoruyko. End-to-end object detection with transformers. In Andrea Vedaldi, Horst Bischof, Thomas Brox, and Jan-Michael Frahm, editors, *Computer Vision – ECCV 2020*, pages 213–229, Cham, 2020. Springer International Publishing.
- [35] Kaiming He, Xiangyu Zhang, Shaoqing Ren, and Jian Sun. Deep residual learning for image recognition. *CoRR*, abs/1512.03385, 2015.
- [36] TorchVision maintainers and contributors. Torchvision: Pytorch’s computer vision library. <https://github.com/pytorch/vision>, 2016.
- [37] Alexey Dosovitskiy, Lucas Beyer, Alexander Kolesnikov, Dirk Weissenborn, Xiaohua Zhai, Thomas Unterthiner, Mostafa Dehghani, Matthias Minderer, Georg Heigold, Sylvain Gelly, Jakob Uszkoreit, and Neil Houlsby. An image is worth 16x16 words: Transformers for image recognition at scale. *CoRR*, abs/2010.11929, 2020.
- [38] Jia Deng, Wei Dong, Richard Socher, Li-Jia Li, Kai Li, and Li Fei-Fei. Imagenet: A large-scale hierarchical image database. In *2009 IEEE Conference on Computer Vision and Pattern Recognition*, pages 248–255, 2009.
- [39] Julius Adebayo, Michael Muelly, Ilaria Liccardi, and Been Kim. Debugging tests for model explanations. In *Proceedings of the 34th International Conference on Neural Information Processing Systems*, NIPS’20, Red Hook, NY, USA, 2020. Curran Associates Inc.
- [40] Dongsheng Luo, Wei Cheng, Dongkuan Xu, Wenchao Yu, Bo Zong, Haifeng Chen, and Xiang Zhang. Parameterized explainer for graph neural network. In *Proceedings of the 34th International Conference on Neural Information Processing Systems*, NIPS’20, Red Hook, NY, USA, 2020. Curran Associates Inc.
- [41] Emanuele Albini, Antonio Rago, Pietro Baroni, and Francesca Toni. Relation-based counterfactual explanations for bayesian network classifiers. In Christian Bessiere, editor, *Proceedings of the Twenty-Ninth International Joint Conference on Artificial Intelligence, IJCAI-20*, pages 451–457. International Joint Conferences on Artificial Intelligence Organization, 7 2020. Main track.
- [42] Yash Goyal, Ziyan Wu, Jan Ernst, Dhruv Batra, Devi Parikh, and Stefan Lee. Counterfactual visual explanations. In Kamalika Chaudhuri and Ruslan Salakhutdinov, editors, *Proceedings of the 36th International Conference on Machine Learning*, volume 97 of *Proceedings of Machine Learning Research*, pages 2376–2384. PMLR, 09–15 Jun 2019.
- [43] Karthikeyan Natesan Ramamurthy, Bhanukiran Vinzamuri, Yunfeng Zhang, and Amit Dhurandhar. Model agnostic multilevel explanations. In *Proceedings of the 34th International Conference on Neural Information Processing Systems*, NIPS’20, Red Hook, NY, USA, 2020. Curran Associates Inc.
- [44] Yifei Zhang, Siyi Gu, James Song, Bo Pan, Guangji Bai, and Liang Zhao. Xai benchmark for visual explanation, 2023.
- [45] Chun-Hao Chang, Elliot Creager, Anna Goldenberg, and David Duvenaud. Explaining image classifiers by counterfactual generation. In *International Conference on Learning Representations*, 2019.
- [46] Yuyi Zhang, Feiran Xu, Jingying Zou, Ovanes L. Petrosian, and Kirill V. Krinkin. Xai evaluation: Evaluating black-box model explanations for prediction. In *2021 II International Conference on Neural Networks and Neurotechnologies (NeuroNT)*, pages 13–16, 2021.

- [47] Umang Bhatt, Adrian Weller, and José M. F. Moura. Evaluating and aggregating feature-based model explanations. In *Proceedings of the Twenty-Ninth International Joint Conference on Artificial Intelligence, IJCAI'20*, 2021.
- [48] Patrick Schwab and Walter Karlen. Cxplain: Causal explanations for model interpretation under uncertainty. In H. Wallach, H. Larochelle, A. Beygelzimer, F. d'Alché-Buc, E. Fox, and R. Garnett, editors, *Advances in Neural Information Processing Systems*, volume 32. Curran Associates, Inc., 2019.
- [49] Michael Chromik and Martin Schuessler. A taxonomy for human subject evaluation of black-box explanations in xai. *Exss-atec@ iui*, 1, 2020.
- [50] Aliasghar Khani, Saeid Asgari Taghanaki, Aditya Sanghi, Ali Mahdavi Amiri, and Ghassan Hamarneh. Slime: Segment like me, 2024.
- [51] Tim Miller. Explanation in artificial intelligence: Insights from the social sciences. *Artificial Intelligence*, 267:1–38, 2019.
- [52] Aditya Ramesh, Mikhail Pavlov, Gabriel Goh, Scott Gray, Chelsea Voss, Alec Radford, Mark Chen, and Ilya Sutskever. Zero-shot text-to-image generation. *CoRR*, abs/2102.12092, 2021.

A Supplementary model evaluations

A.1 ResNet

Evaluation. In Table 4, we detail the quantitative results for the ResNet-101 model, comparing our evaluation with the criteria used for EfficientNetB4 under consistent hyperparameter settings. The review extends to a comparative analysis with EfficientNetB3, focusing on performance under contrastive conditions. The results confirm the EfficientNet results and show that the LIME techniques behave unpredictably in the presence of model noise or prediction shuffle despite different segmentation strategies. This indicates an inherent randomness in the model explanations. The single deletion metric showed that all XAI approaches performed below EfficientNetB4, with DSEG performing slightly better than its counterparts. However, DSEG performed best on other metrics, especially when combined with the SLIME framework, where it showed superior resilience to noise, distinguishing it from alternative methods.

Table 4: **Quantitative summary - classes ResNet-101.** The table presents the metrics consistently with those discussed for EfficientNet.

Domain	Metric	DSEG				SLIC				QS				FS				WS			
		L	S	G	B	L	S	G	B	L	S	G	B	L	S	G	B	L	S	G	B
Correctness	Random Model ↑	18	18	17	16	15	17	18	19	19	20	20	18	18	19	20	17	19	20	20	20
	Random Expl. ↑	18	19	20	19	20	20	18	18	20	18	19	19	20	19	18	20	18	20	19	20
	Single Deletion ↑	4	3	3	5	4	3	4	4	2	1	3	3	4	3	4	4	3	3	3	3
Output Completeness	Preservation ↑	7	9	6	7	8	8	9	8	5	5	5	5	7	5	4	6	8	7	8	6
	Deletion ↑	10	12	9	13	9	9	9	8	6	8	6	7	7	6	6	7	8	8	9	8
Consistency	Noise Stability ↑	8	10	6	6	5	5	5	4	5	5	5	5	3	2	2	2	6	7	8	6
Contrastivity	Preservation ↑	6	12	8	9	5	5	5	5	6	7	8	8	8	6	6	6	6	7	8	8
	Deletion ↑	6	10	7	10	9	8	8	8	5	7	8	7	6	5	5	4	7	6	5	4

Table 5 presents further findings of ResNet. SLIME with DSEG yields the lowest AUC for incremental deletion, whereas Quickshift and Felzenszwalb show the highest. WS produces the smallest superpixels for compactness, contrasting with DSEG’s larger ones. The stability analysis shows that all segmentations are almost at the same level, with SLIC being the best and GLIME the best-performing overall. Echoing EfficientNet’s review, segmentation defines runtime, with DSEG being the most time-consuming. The runtime disparities between the ResNet and EfficientNet models are negligible.

Table 5: **Quantitative summary - numbers ResNet-101.** The table presents the metrics consistently with those discussed for EfficientNet.

Metric	DSEG				SLIC				QS				FS				WS			
	L	S	G	B	L	S	G	B	L	S	G	B	L	S	G	B	L	S	G	B
Incr. Deletion ↓	0.26	0.09	0.11	0.29	0.25	0.26	0.25	0.23	0.44	0.32	0.34	0.40	0.37	0.32	0.37	0.44	0.23	0.26	0.27	0.25
Compactness ↓	0.24	0.20	0.21	0.18	0.15	0.15	0.14	0.15	0.16	0.16	0.16	0.16	0.16	0.18	0.15	0.15	0.13	0.14	0.13	0.13
Rep. Stability ↓	.024	.023	.020	.022	.020	.020	.016	.021	.022	.021	.018	.021	.022	.022	.017	.022	.022	.021	.018	.020
Time ↓	45.7	49.4	48.4	52.3	20.0	17.5	19.7	18.7	26.0	24.9	24.9	26.0	19.4	17.5	19.4	18.7	19.0	17.0	17.5	17.5

A.2 VisionTransformer

Evaluation. Table 6 provides the quantitative results for the VisionTransformer (ViT-384) model, employing settings identical to those used for EfficientNet and ResNet, with ViT processing input sizes of (384x384). The class-specific results within this table align closely with the performances recorded for the other models, further underscoring the effectiveness of DSEG. This consistency in DSEG performance is also evident in the data presented in Table 7. However, the ‘Noise Stability’ metric shows poorer performance for both models than for EfficientNetB4, indicating that ViT and ResNet have greater difficulty when noise enters the input.

We performed all experiments for ResNet and ViT with the same hyperparameters defined for EfficientNetB4. We would like to explicitly point out that the quantitative results could be improved by defining more appropriate hyperparameters for both DSEG and conventional segmentation methods, as no hyperparameter search was performed for a fair comparison.

Table 6: **Quantitative summary - classes ViT-384.** The table presents the metrics consistently with those discussed for EfficientNet.

Domain	Metric	DSEG				SLIC				QS				FS				WS			
		L	S	G	B	L	S	G	B	L	S	G	B	L	S	G	B	L	S	G	B
Correctness	Random Model \uparrow	17	17	17	17	19	19	19	19	18	18	19	18	19	19	19	19	18	19	18	19
	Random Expl. \uparrow	17	19	19	17	20	17	19	19	19	18	20	18	20	18	19	19	17	17	18	18
	Single Deletion \uparrow	8	9	9	9	6	6	6	6	4	4	4	4	4	5	4	4	4	4	3	3
Output Completeness	Preservation \uparrow	7	7	7	7	6	6	7	7	5	5	4	5	6	6	7	7	6	6	5	6
	Deletion \uparrow	14	16	16	16	15	15	15	15	12	12	12	12	14	15	16	15	15	14	14	14
Consistency	Noise Stability \uparrow	7	6	5	6	7	5	6	5	3	4	4	4	4	4	5	3	5	4	4	4
Contrastivity	Preservation \uparrow	10	8	10	9	8	8	9	9	10	9	10	11	8	7	7	8	10	11	10	10
	Deletion \uparrow	11	13	12	13	9	9	9	9	8	7	8	8	8	9	9	8	9	11	11	11

Table 7: **Quantitative summary - numbers ViT-384.** The table presents the metrics consistently with those discussed for EfficientNet.

Metric	DSEG				SLIC				QS				FS				WS			
	L	S	G	B	L	S	G	B	L	S	G	B	L	S	G	B	L	S	G	B
Incr. Deletion \downarrow	0.18	0.14	0.14	0.45	0.21	0.25	0.30	0.25	0.52	0.54	0.54	0.46	0.36	0.37	0.32	0.39	0.36	0.36	0.37	0.35
Compactness \downarrow	0.17	0.17	0.17	0.16	0.12	0.12	0.12	0.12	0.14	0.14	0.13	0.13	0.13	0.12	0.13	0.12	0.11	0.11	0.10	0.11
Rep. Stability \downarrow	.013	.013	.014	.013	.014	.014	.014	.014	.18	.018	.018	.017	.014	.014	.015	.014	.016	.016	.017	.016
Time \downarrow	39.5	43.1	40.3	43.6	13.5	10.9	11.6	11.7	18.6	17.3	17.1	18.3	20.4	15.6	16.3	18.6	17.8	15.1	15.3	16.8

A.3 EfficientNetB4 with depth of two

Evaluation. In Table 8 and Table 9, we present the quantitative comparison between DSEG-LIME ($d = 2$) using EfficientNetB4 and SLIC, as reported in the main paper. The hyperparameter settings were consistent across the evaluations, except for compactness. We established a minimum threshold of 0.05 for values to mitigate the impact of poor segmentation performance, which often resulted in too small segments. Additional segments were utilized to meet this criterion for scenarios with suboptimal segmentation. However, this compactness constraint was not applied to DSEG with depth two since its hierarchical approach naturally yields smaller and more detailed explanations, evident in Table 9. The hierarchical segmentation of $d = 2$ slightly impacts stability, yet the method continues to generate meaningful explanations, as indicated by other metrics. Although our method demonstrated robust performance, it required additional time because the feature attribution process was conducted twice.

Table 8: **Quantitative summary - classes depth two.** The table showcases metrics for EfficientNetB4, specifically at a finer concept granularity; the hierarchical segmentation tree has $d = 2$. Results reported pertain solely to integrating DSEG and SLIC within the scope of the LIME frameworks examined.

Domain	Metric	DSEG				SLIC			
		L	S	G	B	L	S	G	B
Correctness	Random Model \uparrow	16	16	16	16	14	14	14	14
	Random Expl. \uparrow	16	18	18	14	15	19	16	15
	Single Deletion \uparrow	9	10	9	11	8	8	8	8
Output Completeness	Preservation \uparrow	16	13	14	13	16	16	16	16
	Deletion \uparrow	6	10	10	9	7	8	8	8
Consistency	Noise Stability \uparrow	13	14	14	15	14	14	14	14
Contrastivity	Preservation \uparrow	14	12	12	13	9	9	9	9
	Deletion \uparrow	6	6	7	6	9	10	10	10

Table 9: **Quantitative summary - numbers depth two.** The table showcases the numeric values in the same manner as in Table 8 but for numeric values.

Metric	DSEG				SLIC			
	L	S	G	B	L	S	G	B
Incr. Deletion ↓	0.40	0.26	0.15	0.16	0.38	0.31	0.30	0.35
Compactness ↓	0.08	0.12	0.09	0.09	0.13	0.13	0.13	0.13
Rep. Stability ↓	.011	.010	.011	.011	.008	.008	.009	.009
Time ↓	75.2	72.7	73.6	75.0	17.8	18.1	19.5	17.6

Exemplary explanations. DSEG-LIME introduces a hierarchical feature generation approach, allowing users to specify segmentation granularity via tree depth. Figure 4 displays five examples from our evaluation, with the top images showing DSEG’s explanations at a hierarchy depth of one and the bottom row at a depth of two. These explanations demonstrate that deeper hierarchies focus on smaller regions. However, the banana example illustrates a scenario where no further segmentation occurs if the concept, like a banana, lacks sub-components for feature generation, resulting in identical explanations at both depths.

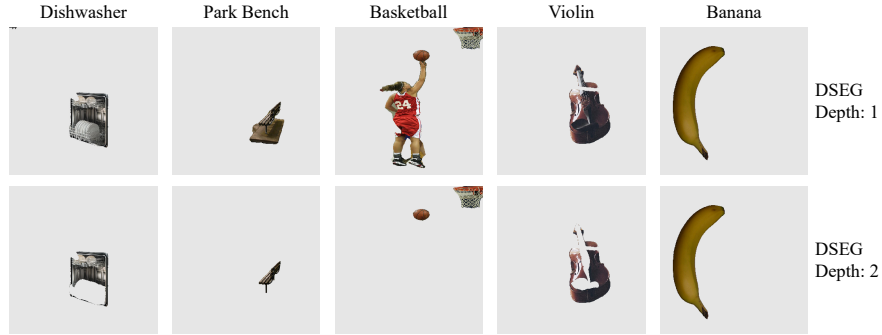


Figure 4: **DSEG depth two.** The figure displays exemplary images from the evaluation dataset, illustrating DSEG explanations at $d = 2$ of hierarchical segmentation. These images serve as complementary examples to the paper’s discussion on the projectile, enhancing the illustration of the concept.

In Figure 5, another instance is explained with DSEG and $d = 2$, showing a black-and-white image of a projectile. Here, we see the corresponding explanation for each stage, starting with the first iteration with the corresponding segmentation map. In the second iteration, we see the segment representing the projectile split into its finer segments - the children nodes of the parent node - with the corresponding explanation below.

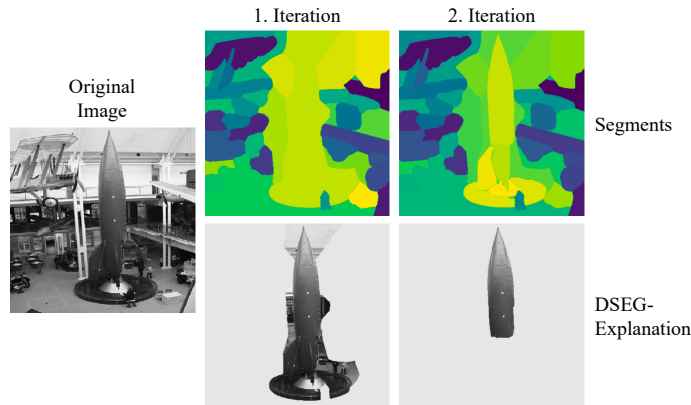


Figure 5: **2nd iteration of DSEG-LIME.** Visualizing DSEG’s explanations of a projectile. It includes the first iteration’s explanation along with its corresponding segmentation map. Additionally, similar details are provided for the second iteration procedure, highlighting the upper part of a projectile as an explanation.

Case study. We examine the case presented in Figure 3, where DSEG initially segments the image into various layers with overlapping features, establishing a segmentation hierarchy through composition. In the first iteration, LIME focuses solely on the segments just beneath the root node - the parent segments that cannot be merged into broader concepts. From this segmentation map, LIME determines the feature importance scores, identifying the airplane as the most crucial element in the image. In the subsequent iteration, illustrated in Figure 6, DSEG generates an additional segmentation map that further divides the airplane into finer components for detailed analysis. The explanation in this phase emphasizes the airplane’s body, suggesting that this concept of the ‘Airliner’ is most significant.



Figure 6: **Airliner explanation with depth two.** The same example as in Figure 3 but with segmentation hierarchy of two for the explanation. This example includes the children nodes of the most significant parent node in the segmentation map for feature importance calculation.

A.4 DETR within DSEG

Evaluation. In Table 10 and Table 11, we conducted the DETR experiments within LIME on an Apple M3 Pro silicon chip. Based on previous results, we evaluate its performance by comparing it to SLIC within LIME. Both experiments were configured with identical parameters, and DETR was implemented for basic panoptic segmentation.

Table 10: **Quantitative summary - classes DETR.** The table showcases metrics for EfficientNetB4, specifically at a finer concept granularity; the hierarchical segmentation tree has a depth of two. Results reported pertain solely to integrating DSEG and SLIC within the scope of the LIME frameworks examined.

Domain	Metric	DSEG				SLIC			
		L	S	G	B	L	S	G	B
Correctness	Random Model \uparrow	15	15	15	15	14	14	14	14
	Random Expl. \uparrow	15	17	19	19	15	19	16	15
	Single Deletion \uparrow	10	10	10	10	8	8	8	8
Output Completeness	Preservation \uparrow	16	16	17	17	16	16	16	16
	Deletion \uparrow	12	12	11	11	7	8	8	8
Consistency	Noise Stability \uparrow	15	12	12	12	14	14	14	14
Contrastivity	Preservation \uparrow	11	11	11	11	9	9	9	9
	Deletion \uparrow	14	14	14	14	9	10	10	10

DETR demonstrates superior performance on the dataset compared to the LIME variants utilizing SLIC. However, like SAM, DETR required more time to complete the segmentation tasks. We are not including the incremental deletion declaration to prevent confusion about the implications of the result. This is because the logit value of the model for the designated class of the image is multiplied by the area of the segment. In the case of DETR, initial evaluations often show that the most significant segment initially classified differs from subsequent classifications when additional segments are included. This difference often leads to specific values being assigned a zero or NaN, which happens when the explanation involves multiplication by zero at the beginning.

Despite its efficacy, the segmentation quality of DETR was generally inferior to that of SAM, as evidenced by less compact explanations. This observation is further supported by the examples in Figure 7. The visualizations reveal that DETR often segments images in ways that do not align with typical *human-recognizable* concepts, highlighting a

Table 11: **Quantitative summary - numbers DETR**. The table showcases the numeric values in the same manner as in Table 10 but for numeric values.

Metric	DSEG				SLIC			
	L	S	G	B	L	S	G	B
Compactness ↓	0.24	0.26	0.26	0.26	0.13	0.13	0.13	0.13
Rep. Stability ↓	.007	.006	.006	.007	.008	.008	.009	.009
Time ↓	41.9	42.6	42.7	42.8	36.1	36.1	34.9	37.0

potential limitation in its practical utility for generating explanatory segments. Moreover, DETR does not support the construction of a segmentation hierarchy, lacking the ability to produce finer and coarser segments, which diminishes its flexibility compared to methods such as SAM.

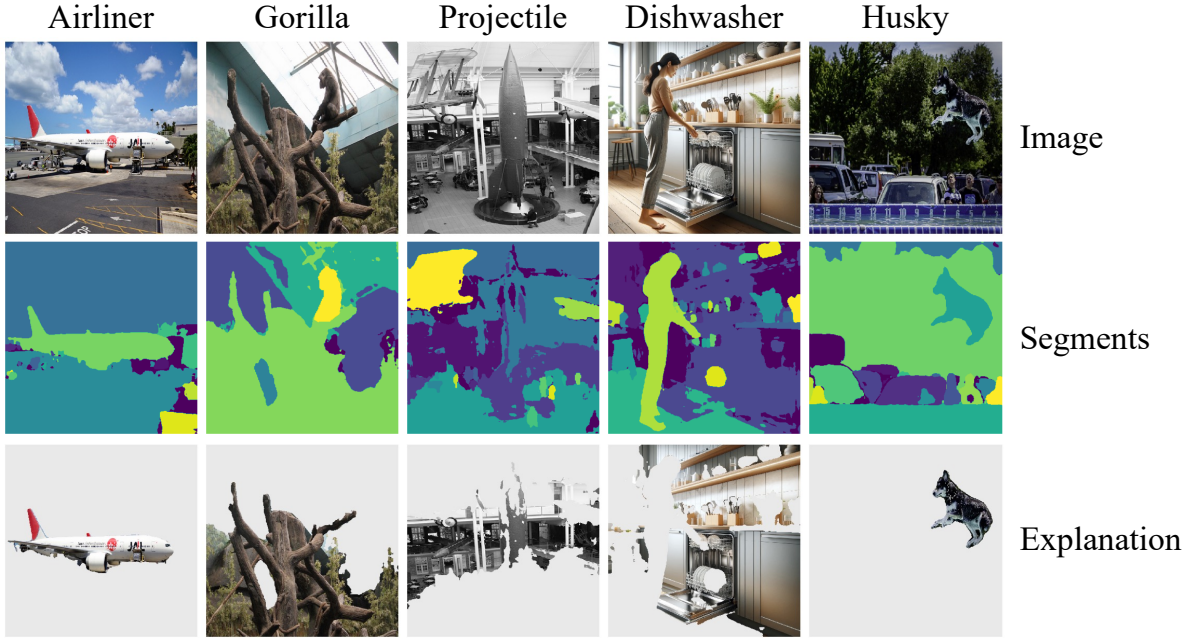


Figure 7: **DETR within DSEG**. The visualization displays five instances with classes from the ImageNet dataset. Each image includes the prediction by EfficientNetB4 as its headline, the segmentation map of DETR, and the corresponding explanation by DETR within LIME.

A.5 Further explanations of DSEG-LIME

Stability of explanations. The stability of imagery explanations using LIME can be linked to the quality of feature segments, as illustrated in Figure 8. This figure presents the segmentation maps generated by various techniques alongside their explanations and coefficient distributions, displayed through an IQR plot over eight runs. Notably, the DSEG technique divides the image into meaningful segments; the gorilla segment, as predicted by the EfficientNetB4 model, is distinctly visible and sharply defined. In contrast, other techniques also identify the gorilla, but less distinctly, showing significant variance in their coefficient distributions. Watershed, while more stable than others, achieves this through overly broad segmentation, creating many large and a few small segments. These findings align with our quantitative evaluation and the described experimental setup.

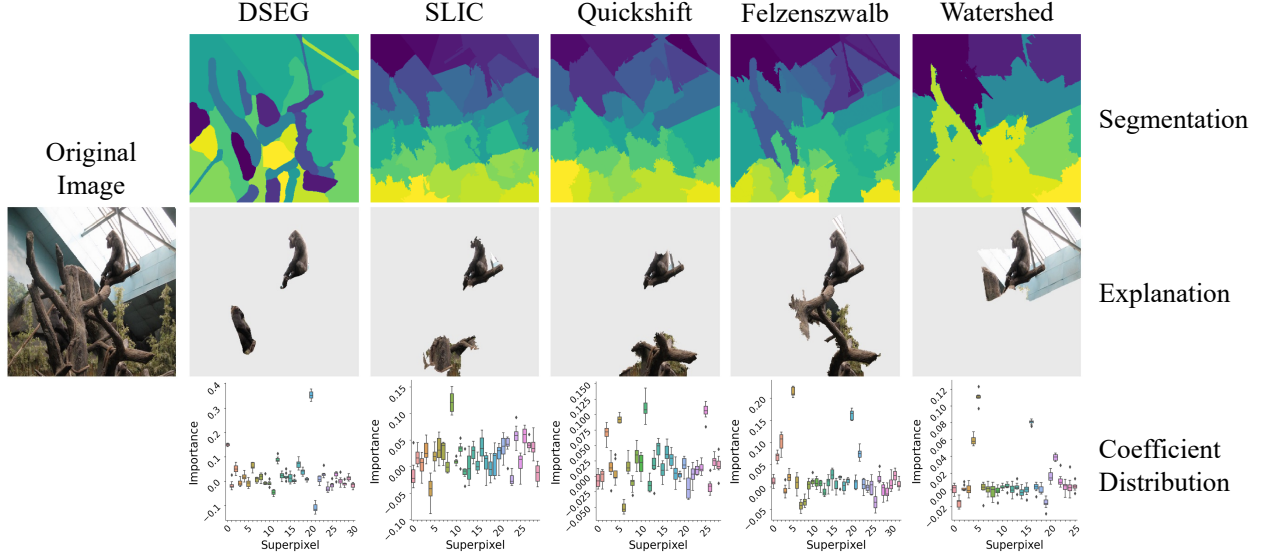


Figure 8: **Segmentation stability.** Illustrating a comparison between DSEG and other segmentation techniques applied in LIME, all utilizing an identical number of samples. DSEG exhibits greater stability compared to other segmentation techniques. Notably, the DSEG explanation distinctly highlights the segment representing a gorilla as the most definitive.

Limitation example of DSEG. The example in Figure 9 shows a complex case of a hermit crab in front of sand, which is hardly detectable. Here, SAM fails to segment the image into meaningful segments, a known issue in the community [50]. In contrast, SLIC can generate segments; thus, LIME can produce an explanation that does not show a complete image.

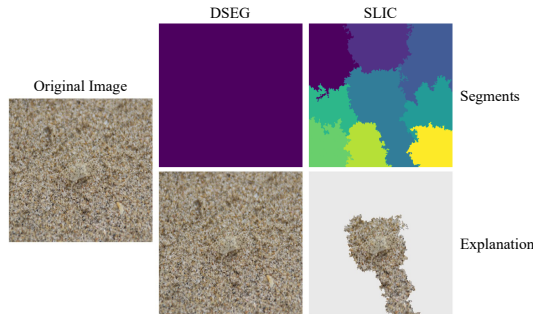


Figure 9: **DSEG fails.** Demonstrating a scenario where DSEG fails to generate meaningful features for explanations (the the whole image is one segment, in contrast to SLIC. The image shows a crab, which the model classifies as a 'hermit crab' ($p = 0.17$), highlighting the effectiveness of SLIC in this context compared to the limitations of DSEG.

Feature attribution maps. In addition to visualizing the n most essential segments for an explanation, feature attribution maps also help the explainee (the person receiving the explanation [51]) to get an idea of which other segments are important for interpreting the result. In these maps, the segments represent the corresponding coefficient of the surrogate model learned within LIME for the specific case. Blue segments are positively associated with the class to be explained, and red segments are negatively associated. The object representing the class is the most unique feature in all three images. We can see this particularly clearly in the image with the airplane, as the other segments have hardly any weight.

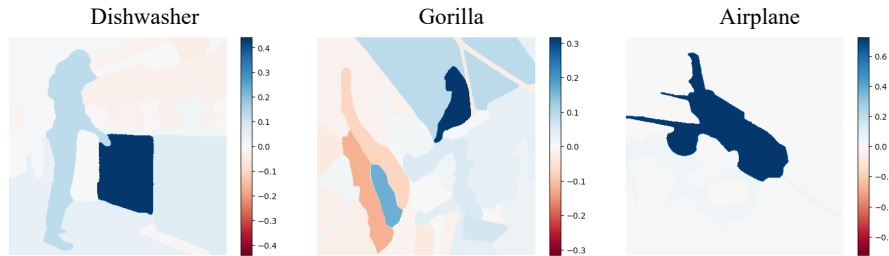


Figure 10: **DSEG attribution maps.** Representation of the feature weights of three different classified images in a feature map, with blue segments indicating positively important and red segments negatively important features in relation to the classified label. The unique blue feature indicates that the class to be explained can be recognized in all three images.

B Dataset and user study

B.1 Dataset

Image selection. As mentioned in Section 5.1, we selected various classes of images from the ImageNet [38] and COCO [33] dataset. Additionally, we created artificial images using the text-to-image model DALL-E [52] to challenge the XAI techniques when facing multiple objects. The dataset for the evaluation comprised 17 real images and three synthetic images. For the synthetic instances, the prompts 'realistic airplane at the airport', 'realistic person running in the park', and 'realistic person in the kitchen in front of a dishwasher' were used, and the corresponding images can be found in Figures 11 and 12.

Explanations. In Figures 11 and 12 we show all 20 images of the dataset used for the evaluation. Each image is accompanied by the prediction of EfficientNetB4 and the explanations within the vanilla LIME framework with all four segmentation approaches and the DSEG variant. The segments shown in the image indicate the positive features of the explanation.















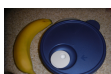






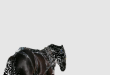








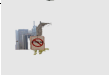














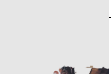

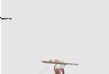
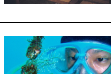
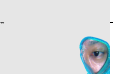
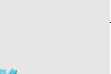
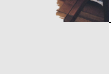
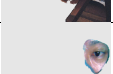
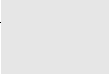
Original Image	Prediction	DSEG	SLIC	QS	FS	WS
	Ski					
	Husky					
	Tennis Racket					
	Banana					
	Horse					
	Street Sign					
	Airplane					
	Projectile					
	Violin					
	Scuba Diver					

Figure 11: **Images 1 - 10.** The first ten examples of the images in the evaluation datasets with the LIME explanations and the corresponding original image with the prediction.








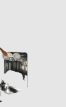

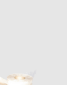
Original Image	Prediction	DSEG	SLIC	QS	FS	WS
	Miniskirt					
	Chihuahua					
	Ice Bear					
	Gorilla					
	Basketball					
	Catamaran					
	Dishwasher					
	Paper Towel					
	CD Player					
	Park Bench					

Figure 12: **Images 11 - 20.** The last examples of the images in the evaluation datasets with the LIME explanations and the corresponding original image with the prediction.

B.2 User study



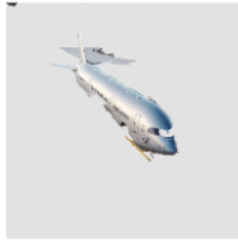


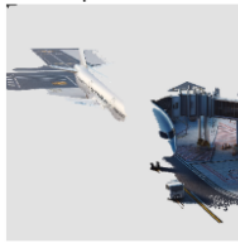
We have carefully examined whether there are any risks for the participants in the study. As they only have to rate images according to their opinion without providing any information of their own, and the images do not show any sensitive content, the overall risk is very low. For the user study conducted through MTurk, we did not select participants with specialized knowledge, as the classes reflect everyday situations. Each participant received compensation of \$4.50 per survey, plus an additional \$2.08 handling fee charged by MTurk and \$1.24 tax. The survey, designed to assess a series of pictures, takes approximately 10 to 15 minutes to complete. The sequence in which the explanations are presented to the participants was randomized to minimize bias. In our study conducted via MTurk, 59 individuals participated, along with an additional 28 people located near our research group who participated at no cost.

Instruction. Participants were tasked with the following question for each instance: 'Please arrange the provided images that best explain the concept [*model's prediction*], ranking them from 1 (least effective) to 5 (most effective).' Each instance was accompanied by DSEG, SLIC, Watershed, Quickshift, Felzenszwalb, and Watershed within the vanilla LIME framework and the hyperparameters discussed in the experimental setup. These are also the resulting

explanations used in the quantitative evaluation of EfficientNetB4. Figure 13 shows an exemplary question of an instance of the user study. The explanations and instances provided to the participants are shown in Figure 11 and Figure 12.

⋮

Please arrange the provided images that best explains the concept **airplane**, ranking them from 1 (least effective) to 5 (most effective). ★

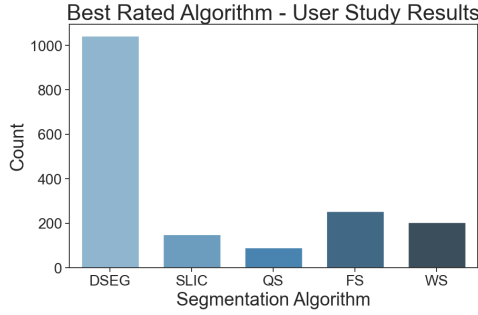
Original Image	Explanation 1	Explanation 2	Explanation 3	Explanation 4	Explanation 5
					

	1	2	3	4	5
Explanation 1	<input type="radio"/>	<input type="radio"/>	<input type="radio"/>	<input type="radio"/>	<input type="radio"/>
Explanation 2	<input type="radio"/>	<input type="radio"/>	<input type="radio"/>	<input type="radio"/>	<input type="radio"/>
Explanation 3	<input type="radio"/>	<input type="radio"/>	<input type="radio"/>	<input type="radio"/>	<input type="radio"/>
Explanation 4	<input type="radio"/>	<input type="radio"/>	<input type="radio"/>	<input type="radio"/>	<input type="radio"/>
Explanation 5	<input type="radio"/>	<input type="radio"/>	<input type="radio"/>	<input type="radio"/>	<input type="radio"/>

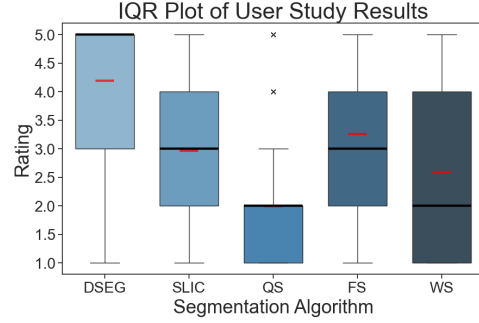
Figure 13: **Exemplary question.** The 'airplane' example is shown in the original image with its five explanations. Below the images, participants can rate the quality of the explanations accordingly.

Results. We show the cumulative maximum ratings in Figure 14a and in Figure 14b the median (in black), the interquartile range (1.5), and the mean (in red) for each segmentation technique. DSEG stands out in the absolute ratings, significantly exceeding the others. Similarly, in Figure 14b, DSEG achieves the highest rating, indicating its superior performance relative to other explanations. Therefore, while DSEG is most frequently rated as the best, it consistently ranks high even when it is not the leading explanation, as the IQR of DSEG shows. Aligned with the quantitative results in Section 5.2, the Quickshift algorithm performs the worst.

Table 12 presents the statistical significance of the user study. Specifically, it lists the t-statistics and p-values for comparisons between DSEG (the baseline method) and other segmentation methods, namely SLIC, QS, FS, and WS. The t-statistics indicate the magnitude of difference between DSEG and each other method, with higher values



(a) **Best rated explanation.** Accumulated number of best-selected explanations within the user study. DSEG was selected as the favorite, followed by Felzenszwalb and Watershed.



(b) **IQR of explanation's ratings.** The IQR plot of the user study ratings is detailed, with the black line indicating the median and the red line representing the mean. This plot shows that DSEG received the highest ratings, while Watershed exhibited the broadest ratings distribution.

Figure 14: **User study results.** The user study ratings are visualized in two distinct figures, each employing a different form of data representation. In both visualizations, DSEG consistently outperforms the other techniques.

representing greater differences. The corresponding p-values demonstrate the probability that these observed differences are due to random chance, with lower values indicating stronger statistical significance.

Table 12: **User study statistical results.** This table summarizes the statistical significance of user study results for each segmentation approach. The t-statistics and p-values indicate the comparison between DSEG and other methods. Extremely low p-values suggest strong statistical significance.

Metric	DSEG	SLIC	QS	FS	WS
t-statistics \uparrow	–	20.01	49.39	20.89	33.15
p-values \downarrow	–	8.0e-143	< 2.2e-308	1.2e-86	3.3e-187

In this context, the null hypothesis (H_0) posits that there is no significant difference between the performance of DSEG and the other segmentation methods. Given the extremely low p-values (e.g., 8.0e-143 for SLIC and < 2.2e-308 for QS), we can reject the null hypothesis with high confidence. The significance level of 99.9% ($\alpha = 0.001$) further strengthens this conclusion, as all p-values are well below this threshold, indicating that the observed differences are highly unlikely to have occurred by chance and thus are statistically significant.